

Smart Corrosion Inhibition of Mild Steel Using Mesoporous Silica Nanocontainers Loaded with Molybdate

M. Yeganeh*, S. M. Marashi and N. Mohammadi

Department of Materials Science and Engineering, Faculty of Engineering, Shahid Chamran University of Ahvaz, Ahvaz, Iran.

(*) Corresponding author: m.yeganeh@scu.ac.ir

(Received: 20 March 2017 and Accepted: 14 October 2017)

Abstract

In this research, mesoporous silica was served as the host of molybdate (corrosion inhibitor). The loaded mesoporous silica was dispersed in a paint matrix. The composite was then coated on the carbon steel surface. Polarization and electrochemical impedance spectroscopy (EIS) tests showed that the corrosion resistance of the scratched paint containing molybdate loaded mesoporous silica was better than the one without it or neat paint at near neutral pH. Charge transfer resistance regarding inhibitor loaded mesoporous silica showed a higher value in comparison with unloaded one. This parameter for the coating with inhibitor loaded mesoporous silica at the higher pH recorded $589300 \Omega \cdot \text{cm}^2$, while it was $209100 \Omega \cdot \text{cm}^2$ for un-loaded mesoporous silica. On the other hand, scanning electron microscopy (SEM) studies showed the release of corrosion inhibitor in the scratch zone which was due to the pH-sensitive release of corrosion inhibitor in the corrosive media.

Keywords: Mesoporous silica, Molybdate, Corrosion inhibitor, Release, Smart corrosion protection.

1. INTRODUCTION

A lot of metals and alloys are susceptible to corrosion damage. A conventional technique to improve their corrosion resistance is the application of polymer coating. However, all polymeric coatings are practically permeable to corrosive species such as chloride ions, oxygen, and water molecules [1–5].

The embedded inorganic fillers into the polymeric matrix could lead to the enhancement of anti-corrosion property of the organic coatings [4, 6]. In the recent years, the applied inorganic fillers have been served as the host of corrosion inhibitor in the coatings. These hosts consist of micro or nanocapsules [7, 8], ion exchange substances [9–11], layer-by-layer polyelectrolyte shells [12–14], porous materials [15–17], and etc. Mesoporous silica with the controlled porous structure has been applied as a porous

corrosion inhibitor host [15, 18–20]. This material has hexagonal and uniform cylindrical pores with the internal diameter in the range of 2-50 nm, high surface area ($700\text{--}1500 \text{ m}^2 \text{ g}^{-1}$), large pore volume ($1 \text{ cm}^3 \text{ g}^{-1}$), high chemical and thermal stability, and easy functionalization [21]. Borisova et al. have loaded 1H-benzotriazole (BTA) in the mesoporous silica by reduction in the pressure during the loading of inhibitor. They embedded these loaded containers in the sol-gel films. The results showed reasonable loading of the nanocontainers and an improvement in the corrosion resistance of AA2024 aluminum alloy in 0.1 M NaCl by the application of an anti-corrosive system consisting of a $\text{SiO}_x/\text{ZrO}_x$ film containing BTA-loaded mesoporous silica. Besides, the results showed the pH-dependent release of

inhibitor from mesoporous silica [22]. In another work which was performed by Chen et al., BTA was loaded in the hollow mesoporous silica spheres. The results illustrated that there was almost no leakage of BTA from mesoporous silica in neutral solution, while in alkaline solution BTA released very quickly, and the release rate increased with increasing pH values [15]. In other works, researchers loaded various kinds of inhibitor including organic [23–25], inorganic [26, 27], and eco-friendly types [25] in the mesoporous silica by direct loading, functionalization process, or using polyelectrolytes.

In this work, we have used functionalized mesoporous silica (SBA type) and applied as a pH-sensitive in corrosive media. Functionalized mesoporous silica as the nano container of molybdate corrosion inhibitor could hinder the corrosion process. The effect of loaded mesoporous silica with inhibitor on the corrosion behavior of carbon steel was examined. Although, the effect of pH change on the corrosion behavior of composite coatings was investigated.

2. EXPERIMENTAL DETAILS

2.1. Materials

Mesoporous silica powders were synthesized by mixing surfactant molecules such as hexadecyltrimethylammonium bromide (CTAB) and a silica precursor (tetraethylorthosilicate, TEOS) [27]. Figure 1 shows the schematic procedure of functionalizing the mesoporous silica (MS or C). The as synthesized product was then refluxed in an acidic 2-propanol for 2 h to remove the CTAB. The initial mesoporous silica (Figure 1a) was functionalized by 1-(2-aminoethyl) 3-aminopropyltrimethoxysilane ($\geq 97.0\%$; TCI America) in the toluene (anhydrous, 99.8%; Sigma-Aldrich) and heated up to 400 K in an inert ambient. In this stage, dropwise addition of 5 mL silane group to 1.5 g was performed. Then, the reactants

were stirred and refluxed overnight in an inert ambient. The obtained powders were filtered and washed with ethanol ($\geq 99.0\%$; VWR) (Figure 1b). In the next step, 0.2 g of FeCl_3 (anhydrous, powder, $\geq 99.99\%$; Sigma-Aldrich) was incorporated in the 1 g functionalized mesoporous silica in the propanol ($\geq 99.7\%$ Analar NORMAPUR; VWR) solution at ambient temperature for 3 h. The obtained powder from filtration and washing by ethanol shows in Figure 1c. Finally; the corrosion inhibitor adsorption was carried out. To evaluate the theoretical maximum loading capacity of mesoporous silica for loading molybdate with the diameter of 0.246 nm, the total surface of mesoporous silica powders is divided to the molybdate ion surface area. Therefore, the maximum theoretical loading capacity is 1.26 g (molybdate)/1 g (mesoporous silica). The experimental loading is around one-third of the maximum, because of the occupied surface of mesoporous silica by functionalized groups. The obtained material denoted as MSInh or D (Figure 1d).

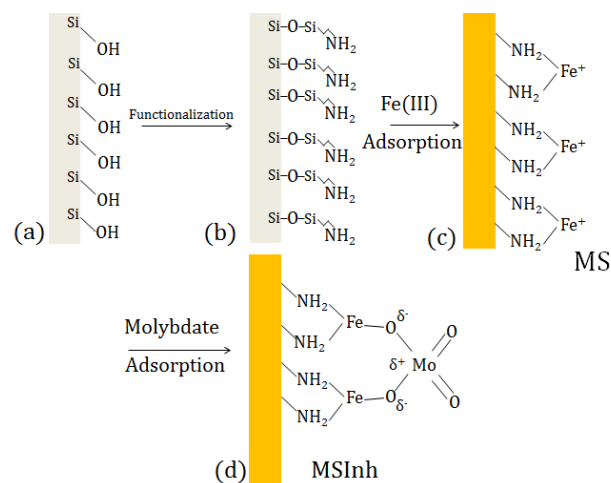


Figure 1. Schematic of loading sodium molybdate corrosion inhibitor into the mesoporous silica: (a) mesoporous silica (MS), (b) functionalization of mesoporous silica by silane group, (c) adsorption of FeCl_3 , and (d) adsorption of the corrosion inhibitor (MSInh).

2.2. Methods

The size and the morphology of MS and MSInh were studied with a high-resolution scanning electron microscope (CamScan Mira, 40 kV) and a transmission electron microscope (TEM Tecnai G2 F30 at 300 kV).

The values of the specific surface area, the average pore diameter, and the pore volume were obtained using N_2 adsorption-desorption isotherms (BELSORP mini-II). The specific surface area was calculated from the adsorption isotherm data in the low-pressure range using the Brunauer-Emmett-Teller (BET) method. The average pore diameter and the pore volume were determined using the Barret-Joyner-Halenda (BJH) method. Fourier transforms infrared spectroscopy

(FT-IR) analysis was also performed in the range of 4000 cm^{-1} to 500 cm^{-1} by Nicolet IR 100 using KBr disk.

To measure the amount of corrosion inhibitor released from MSInh at different pH, 0.05 g MSInh powders were suspended in 10 ml water with pHs of 2, 8, and 14 adjusted by HCl and NaOH. The amount of molybdate ion in the solution was characterized after 3 days by inductively coupled plasma optical emission spectrometry (ICP-OES) model Varian VISTA-MPX.

To investigate the release property of mesoporous silica in the corrosive environment, two composites containing 5 wt. % of these particles (mesoporous silica with (MSInh) and without adsorbed molybdate (MS)) are embedded in the epoxy-paint resin (1001) with epoxy equivalent weight of 450-550 was mixed with a reactive diluent, and these composites were coated on the carbon steel plates. The resulted composite polymers containing MS or MSInh were coated to the steel plates by a film applicator with a thickness of $100 \pm 3\text{ }\mu\text{m}$ measured by an Elcometer 4563 coating thickness meter. Finally, the samples were

dried at $50\text{ }^\circ\text{C}$ for 4 h. Before corrosion tests, the surface of coatings was scratched by a needle. Then, coated steels containing inhibitor loaded mesoporous silica, unloaded mesoporous silica and no mesoporous silica (neat paint) were submerged in the 0.05 (pH=6.4) and 0.15 (pH=5.9) M NaCl (99.5%; Merck) for 3 days.

The electrochemical measurements were carried out in a standard electrochemical cell with a steel plate coated with paint, paint-loaded mesoporous silica with molybdate composite and paint-unloaded mesoporous silica composite as working electrode with an exposed area of 1 cm^2 . Also in these corrosion tests, the surfaces of coatings were scratched with a needle by diameter of $100\text{ }\mu\text{m}$ and the length of 1 cm. A Pt plate served as the counter electrode, while a Saturated Calomel Electrode (SCE) was taken as a reference electrode.

EIS measurements were conducted at the open circuit potential by immersing a sample into the solution for 20–30 min. The AC amplitude was 5 mV, and the frequency was set in the range of 100 kHz to 0.01 Hz using a 1260 Solarton frequency response analyzer (FRA). The ZView3 software was used to analyze the EIS data. All the measurements were done on an EG&G potentiostat-galvanostat 273A model equipment controlled by the software M352. All electrochemical tests were performed at least three times to ensure data output accuracy.

3. RESULTS AND DISCUSSION

The SEM morphology of mesoporous silica is shown in Figure 2(a). The outer diameter of each mesoporous silica tube varies from about 50 to 300 nm, while their length was more than one micrometer. Figure 2(b) presents the TEM morphology of mesoporous silica with hexagonal pores in the range of 4-5 nm.

Table 1 provides information about the specific surface area, average pore diameter,

and pore volume of the mesoporous silica (MS or C) and inhibitor loaded functionalized mesoporous silica (MSInh or D). As shown in this table, specific surface area, pore volume, and pore diameter size decreased after functionalization due to the adsorption of molybdate ions on the surface of mesoporous silica.

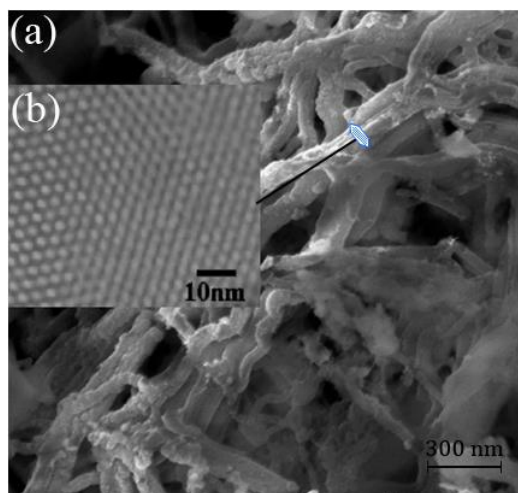


Figure 2. (a) SEM and (b) TEM micrograph of mesoporous silica.

Table 1. Specific surface area, average pore diameter, and pore volume of the MS (C) and MSInh (D).

specimen	Specific surface area ($\text{m}^2 \text{g}^{-1}$)	Pore volume ($\text{cm}^3 \text{g}^{-1}$)	average pore diameter (nm)
MS	776.2	0.84	4.33
MSInh	460.5	0.48	3.8

Figure 3 depicts the FTIR spectra of the MSInh after immersion in water with different pH values for 3 days. It can be seen from this figure that in addition to Si-O (860 cm^{-1}) and Si-O-Si bonds (1080 cm^{-1}), the MoO peaks (886 cm^{-1}) were disappeared at pH ~14 which were due to the deterioration of the MS structures and therefore the release

of molybdate from MSInh in an alkaline media. Furthermore, MSInh maintained their structure in the acidic (pH~2) and near neutral (pH~8) media which confirms that the release of molybdate was because of the deterioration of MSInh structure at high pH.

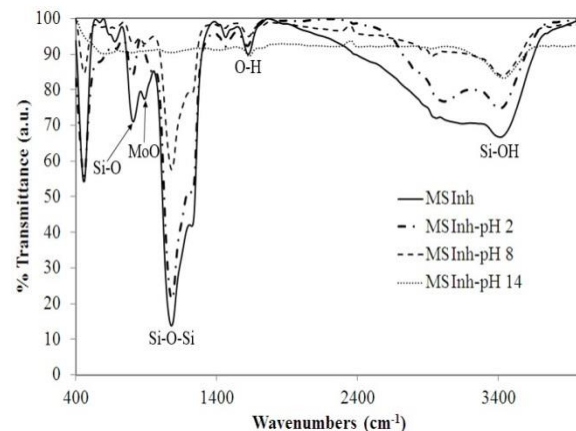


Figure 3. FTIR spectra of MSInh before and after immersion in water with pH values of pH 2, 8, and 14.

Table 2 listed the release content of molybdate in the various acidic, basic, and neutral media.

As seen in this table, the amount of molybdate release in the alkaline ambient showed higher values than acidic one. It was probably due to the surface potential of powders in the solution.

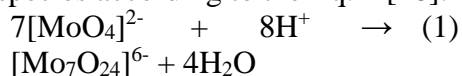
At pH values different from neutral, mesoporous silica particles and inhibitor ions have the same charge. This leads to larger electrostatic repulsion forces and faster release observed. The mesoporous silica particles at the alkaline pH have a negative charge [22]. Therefore, it could help electrostatic repulsion forces between the mesoporous silica and molybdate ions and faster release in these ambient could be observed.

At the acidic conditions, the mesoporous silica particles have a positive charge while the charge of molybdate ions remains negative. Therefore, the attraction between them causes lower release [22].

Table 2. Release content of molybdate in the various acidic, basic, and neutral ambient.

Ambient pH	Total Molybdate concentration (ppm)
pH=1	0.86
pH=2	1.26
pH=5.9	35
pH=6.4	91
pH=7.5	98
pH=8	105
pH=8.2	127
pH=13	490
pH=14	320

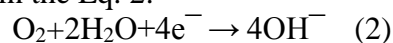
On the other hand, the polymerization of molybdate species begins below pH 6 by the formation of heptamolybdate ($\text{Mo}_7\text{O}_{24}^{6-}$) species according to the Eq. 1 [18]:



Therefore, the release property of molybdate from mesoporous silica at the acidic pH is declined due to the formation of polymolybdate species [18]. Larger polymeric molybdate species may precipitate on the mesoporous silica powders and do not participate completely in the solution. Therefore, the amount of molybdate in the solution becomes lower in comparison with higher pH [18].

Mesoporous silica nanocarrier could react with OH^- ions, and therefore, cathodic reaction in the near neutral media diminished. As a result, the rate of anodic reaction and total corrosion rate decreased. In these solutions, the probable cathodic reaction is

the reduction of oxygen to hydroxyl as shown in the Eq. 2:



As the OH^- ions form in the cathodic sites, the reaction with mesoporous silica nanocarrier occurs and therefore, the content of OH^- ions is decreased. Thus, a release of the corrosion inhibitor in response to pH changes in these environments is expected without the need for an additional polyelectrolyte shell systems [28–30]. Therefore, the near neutral environment for the test of corrosion response of mesoporous silica is a good choice. On the other hand, the molybdate possess the better performance in these media ($\text{pH} > 6$). In addition, the higher release of molybdate at the alkaline media may cause a negative effect on the corrosion protection. Therefore, pH=6.4 (0.05 M NaCl) was chosen for the corrosion tests. To realize pH sensitivity of inhibitor loaded mesoporous silica, the corrosion tests were compared at another pH such as 5.9. It is expected that the corrosion inhibition of molybdate at pH=5.9 shows the lower protection compared to inhibition at pHs above 6. On the other hand, in the 0.15 M NaCl, dramatic changes can be seen in the corrosion behavior of the coatings. This variation related to the corrosion resistance of coatings could be attributed to release property of molybdate from mesoporous silica at the various pHs. As stated above, the release of molybdate at low pH is limited by the electrostatic behavior of powders surface and inherent properties of molybdate at pHs lower than 6. In other word, the molybdate ions could not release sufficiently and, therefore cannot protect the surface of steel at this pH adequately.

Figure 4 presents the EIS curves regarding the scratched samples in the 0.05 (pH 6.4) and 0.15 (pH 5.9) M NaCl after stabilizing OCP about 1 h.

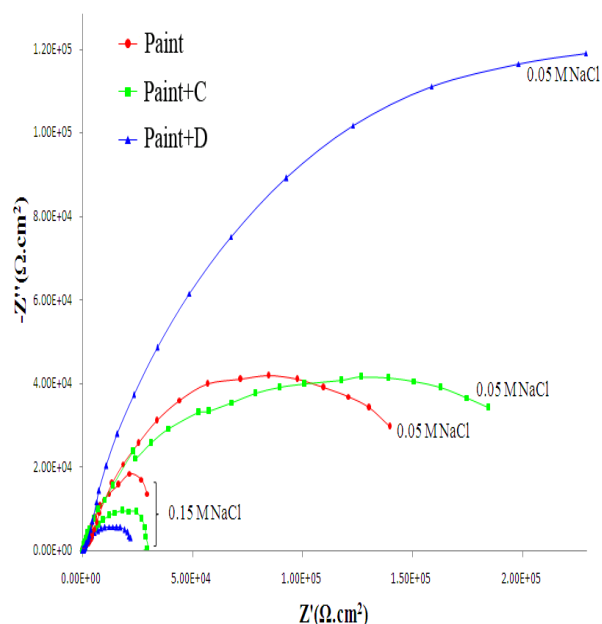


Figure 4. Nyquist plots of paint, paint+ mesoporous silica (C), and paint+ inhibitor loaded mesoporous silica (D) in the 0.05 and 0.15 M NaCl after 1 h of immersion.

The equivalent circuit for these impedance plots is shown in Figure 5.

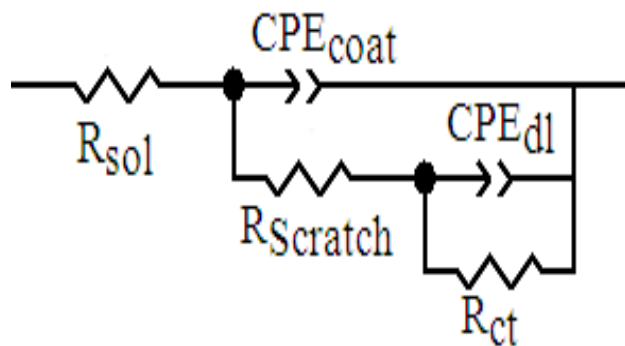


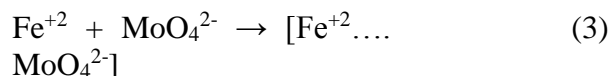
Figure 5. Equivalent circuit for EIS data.

In this model, R_{sol} , R_{ct} , and $R_{scratch}$ are the solution, charge transfer, and scratch resistance, respectively. CPE was used instead of a pure capacitance accounting for a non-ideal capacitive response of the interface. The impedance of a CPE is equal to $[Q(j\omega)^n]^{-1}$, where Q is the constant corresponding to the interfacial capacitance, j is the imaginary number, ω is the angular frequency, and n is an exponential factor in

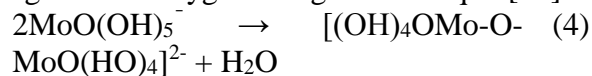
the range between 0 and 1. A value of 1 is related to an ideal capacitor and a value of 0 describes an ideal resistor [31, 32].

CPE_{coat} and CPE_{dl} are related to the paint and electrical double layer. R_{ct} is the resistance of the faradic charge transfers in parallel with a CPE_{dl} . R_{ct} presents the corrosion rate of a metal in a corrosive ambient. The larger R_{ct} of a material becomes, the slower the corrosion rate gets [31].

The obtained values by Zview3 are listed in table 3. As seen in this table, R_{ct} for the paint+D (MSInh) was 589300 $\Omega \cdot cm^2$ in 0.05 M NaCl, while it was 209100 and 167360 $\Omega \cdot cm^2$ for paint+C (MS) and neat coating, respectively. The higher R_{ct} for the paint with loaded inhibitor in the mesoporous silica could be explained by the release of molybdate into the scratch zone [26]. However, as can be observed R_{ct} at the 0.15 M NaCl (pH=5.9) did not differ significantly. It was mainly due to lower release of molybdate at this pH. MoO_4^{2-} can react with Fe^{+2} to form a protective film when molybdate is added to the ambient according to the Eq. 3 [21]:



Furthermore, the reacted molybdate with protons will be coordinated with water molecules to form $MoO(OH)^5-$. In the next step, these species could polymerize to organize an oxygen-bridge ion as Eq. 4 [19]:



The $[(OH)_4OMo-O-MoO(HO)_4]^{2-}$ ions react with the empty orbit d of Fe in the steel to form a complex [21]. Then these complexes adsorb on the steel surface and disrupt charge transfer to inhibit the corrosion reaction.

Also, for the lower pH solution, the coating with the inhibitor loaded mesoporous silica

had the lowest R_{ct} . As mentioned, the lower release of molybdate in this pH is a key factor for higher corrosion rate of steel surface.

Figure 6a depicts the Mo map of the scratched surface at pH=6.4. As seen in this map, the Mo (from molybdate) could release from the paint and distribute on the scratched zone. This demonstrates the ability of mesoporous silica to release corrosion inhibitor in the corrosion sites.

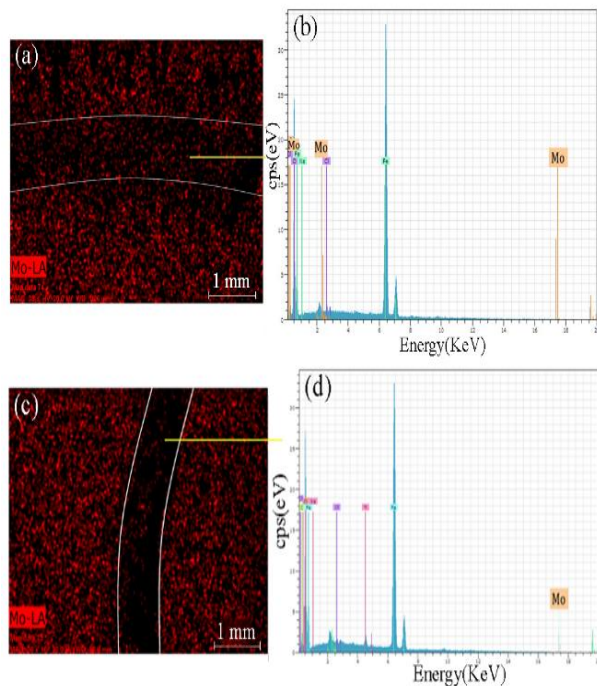


Figure 6. (a) EDX map of scratched zone (0.05 M NaCl), (b) EDX analysis of scratch zone (0.05 M NaCl), (c) EDX map of scratched zone (0.15 M NaCl), and (d) EDX analysis of scratch zone (0.15 M NaCl).

Figure 6b shows the EDX plot of the corroded area. There were Mo peaks in the corroded area, which is a proof of release and adsorbing molybdate on the steel surface in the chloride media. This indicates the

adsorption and reaction of molybdate anions on the carbon steel surface and the formation of a protective layer. Figure 5c presents the Mo map regarding the scratched surface at the pH=5.9. Lower amount of released molybdate in this scratch is seen clearly. Figure 6d shows that the EDX peaks of the corroded surface at the pH=5.9 had the lowest amount of Mo, which is in agreement with the previous results.

4. CONCLUSION

In this research, the effect of loading a corrosion inhibitor into the mesoporous silica was studied. PH-sensitive release of molybdate ions from functionalized mesoporous silica was investigated by several methods. The results showed that molybdate release at alkaline media possessed the highest value, while it had the lowest in the acidic one.

Corrosion inhibition of this system was studied at the pH=6.4 and 5.9. Paint coating which owned the inhibitor loaded into the mesoporous silica showed the highest corrosion resistance in the 0.05 M NaCl (pH=6.4).

Charge transfer resistance regarding loaded inhibitor possessed about three times greater than the un-loaded one at pH of 6.4. It was due to the adsorption of released molybdate from mesoporous silica on the scratched surface and the formation of protective products. On the other hand, molybdate could not protect the surface at pH of 5.9 compared to pH of 6.4. It was mainly due to the lower release of molybdate in the corrosive solution at this pH. Besides, the molybdate could release higher amount into the artificial scratch in the paint coating at the pH of 5.9.

Table 3. Data obtained by ZView3 simulation for paint, paint+ mesoporous silica (C), and paint+ inhibitor loaded mesoporous silica (D) in the 0.05 M NaCl.

%NaCl	sample	R _{sol} (Ω .cm ²)	CPE _{coat} (S-s ⁿ)	R _{Scratch} (Ω .cm ²)	R _{ct} (Ω .cm ²)	CPE _{dl} (S-s ⁿ)	χ^2
0.05 M	Paint	100	7.4E-7	20890	167360	5.2E-7	0.01
	Paint+C	102	2.3E-7	39800	209100	5.3E-6	0.01
	Paint+D	95	1.47E-7	40100	589300	3E-6	0.001
0.15 M	Paint	30	1.36E-5	1297	32400	6.5E-6	0.01
	Paint+C	35	1.48E-5	5217	25900	8.7E-6	0.003
	Paint+D	32	2.3E-5	1900	19600	2.9E-6	0.001

REFERENCES

1. Khramov, A. N., Voevodin N. N., Balbyshev, V. N., Mantz, R. A., (2005) "Sol-gel-derived corrosion-protective coatings with controllable release of incorporated organic corrosion inhibitors," *Thin Solid Films.*, 483: 191–196.
2. Tedim, J., Poznyak, S. K., Kuznetsova, A., Raps, D., Hack, T., Zheludkevich, M. L., Ferreira M. G. S., (2010) "Enhancement of active corrosion protection via combination of inhibitor-loaded nanocontainers," *ACS Appl. Mater. Interfaces.*, 2: 1528–1535.
3. Khramov, A. N., Voevodin, N. N., Balbyshev V. N., Donley M. S., (2004) "Hybrid organo-ceramic corrosion protection coatings with encapsulated organic corrosion inhibitors," *Thin Solid Films.*, 447: 549–557.
4. Abdullayev, E., Lvov, Y., (2010) "Clay nanotubes for corrosion inhibitor encapsulation: release control with end stoppers," *J. Mater. Chem.*, 20: 6681–6687.
5. Zheludkevich, M. L., Poznyak, S. K., Rodrigues, L. M., Raps, D., Hack, T., Dick, L. F., Nunes, T., Ferreira, M. G. S., (2010) "Active protection coatings with layered double hydroxide nanocontainers of corrosion inhibitor," *Corros. Sci.*, 52: 602–611.
6. Lvov, Y. M., Shchukin, D. G., Mohwald, H., Price, R. R., (2008) "Halloysite clay nanotubes for controlled release of protective agents," *ACS Nano.*, 2: 814–820.
7. Buchheit, R. G., Guan, H., Mahajanam, S., Wong, F., (2003) "Active corrosion protection and corrosion sensing in chromate-free organic coatings," *Prog. Org. Coatings.*, 47: 174–182.
8. Mahajanam, S. P. V., Buchheit, R. G., (2008) "Characterization of inhibitor release from Zn-Al-[V₁₀O₂₈] 6-hydroxycalcite pigments and corrosion protection from hydrotalcite-pigmented epoxy coatings," *Corrosion.*, 64: 230–240.
9. Rammelt, U., Duc, L. M., Plieth, W., (2005) "Improvement of protection performance of polypyrrole by dopant anions," *J. Appl. Electrochem.*, 35: 1225–1230.
10. Zheludkevich, M. L., Shchukin D. G., Yasakau, K. A., Möhwald, H., Ferreira, M. G. S., (2007) "Anticorrosion coatings with self-healing effect based on nanocontainers impregnated with corrosion inhibitor," *Chem. Mater.*, 19: 402–411.
11. Walczak M., (2007) "Release studies on mesoporous microcapsules for new corrosion protection systems", VDM Verlag, Germany.
12. Yokoi, T., Tatsumi, T., Yoshitake, H., (2004) "Fe³⁺ coordinated to amino-functionalized MCM-41: an adsorbent for the toxic oxyanions with high capacity, resistibility to inhibiting anions, and reusability after a simple treatment," *J. Colloid Interface Sci.*, 274: 451–457.
13. Cho, Y., Shi, R., Ivanisevic, A., Ben Borgens, R., (2009) "A mesoporous silica nanosphere-based drug delivery system using an electrically conducting polymer," *Nanotechnology.*, 20: 275102.
14. Slowing, I. I., Trewyn, B. G., Giri, S., Lin, V., (2007) "Mesoporous silica nanoparticles for drug delivery and biosensing applications," *Adv. Funct. Mater.*, 17: 1225–1236.
15. Chen, T., Fu, J., (2012) "pH-responsive nanovalves based on hollow mesoporous silica spheres for controlled release of corrosion inhibitor," *Nanotechnology.*, 23: 235605.
16. Yoshitake, H., (2007) "Functionalization of periodic mesoporous silica and its application to the adsorption of toxic anions", Imperial College Press, Singapore.

17. Al-Othman, Z. A., (2006) "*Synthesis, modification, and application of mesoporous materials based on MCM-41*", Ph.D. Thesis: Oklahoma State University.
18. Zhao, J. M., Zuo, Y., (2002) "The effects of molybdate and dichromate anions on pit propagation of mild steel in bicarbonate solution containing Cl^- ," *Corros. Sci.*, 44: 2119–2130.
19. Bolouki, A., Rashidi, L., Vasheghani-Farahani, E., Piravi-Vanak, Z., (2015) "Study of Mesoporous Silica Nanoparticles as Nanocarriers for Sustained Release of Curcumin," *Int. J. Nanosci. Nanotechnol.*, 11: 139–146.
20. Yeganeh, M., Saremi, M., (2014) "Corrosion Behavior of Polypyrrole/Mesoporous Silica Nanocontainers Coatings on the Mild Steel," *Int. J. Nanosci. Nanotechnol.*, 10: 111–116.
21. Qu, Q., Li, L., Jiang, S., Bai, W., Ding, Z., (2009) "Effect of sodium molybdate on the corrosion behavior of cold rolled steel in peracetic acid solution," *J. Appl. Electrochem.*, 39: 569–576.
22. Borisova, D., Möhwald, H., Shchukin, D. G., (2011) "Mesoporous silica nanoparticles for active corrosion protection," *ACS Nano.*, 5: 1939–1946.
23. Mohammadnezhad G., Abad S., Soltani R., Dinari M., (2017) "Study on thermal, mechanical and adsorption properties of amine-functionalized MCM-41/PMMA and MCM-41/PMMA nanocomposites prepared by ultrasonic irradiation," *Ultrason. Sonochem.*, 39: 765–773.
24. Falcón, J. M., Otubo, L. M., Aoki, I. V., (2016) "Highly ordered mesoporous silica loaded with dodecylamine for smart anticorrosion coatings," *Surf. Coatings Technol.*, 303: 319–329.
25. Hollamby, M. J., Fix, D., Dönch, I., Borisova, D., Möhwald, H., Shchukin, D., (2011) "Hybrid polyester coating incorporating functionalized mesoporous carriers for the holistic protection of steel surfaces," *Adv. Mater.*, 23: 1361–1365.
26. Yeganeh, M., Keyvani, A., (2016) "The effect of mesoporous silica nanocontainers incorporation on the corrosion behavior of scratched polymer coatings," *Prog. Org. Coatings.*, 90: 296–303.
27. Keyvani, A., Yeganeh, M., Rezaeyan, H., (2017) "Application of mesoporous silica nanocontainers as an intelligent host of molybdate corrosion inhibitor embedded in the epoxy coated steel," *Prog. Nat. Sci. Mater. Int.*, 27: 261–267.
28. Shchukin, D. G., Zheludkevich, M., Yasakau, K., Lamaka, S., Ferreira, M. G. S., Möhwald, H., (2006) "Layer-by-Layer assembled nanocontainers for self-healing corrosion protection," *Adv. Mater.* 18: 1672–1678.
29. Andreeva, D. V., Skorb, E. V., Shchukin, D. G., (2010) "Layer-by-layer polyelectrolyte/inhibitor nanostructures for metal corrosion protection," *ACS Appl. Mater. Interfaces.*, 2: 1954–1962.
30. Zaarei, D., Sharif, F., Kassirha, S. M., Moazzami Gudarzi, M., (2010) "Preparation and Evaluation of Epoxy-Clay Nanocomposite Coatings for Corrosion Protection," *Int. J. Nanosci. Nanotechnol.*, 6: 126–136.
31. Dhak, P., Dhak, D., Das, M., Pramanik, K., Pramanik, P., (2009) "Impedance spectroscopy study of LaMnO_3 modified BaTiO_3 ceramics," *Mater. Sci. Eng. B.*, 164: 165–171.
32. Yeganeh, M., Eskandari, M., Alavi-Zaree, S. R., (2017) "A Comparison Between Corrosion Behaviors of Fine-Grained and Coarse-Grained Structures of High-Mn Steel in NaCl Solution," *J. Mater. Eng. Perform.*, 26: 2484–2490.